

Article

High Step-up Voltage Gain Converter with Ripple-free Input Current for Renewable Energy Sources

Zhang-yong Chen ^{1,2*} and Yong Chen ^{1,2}

1 School of Energy Science and Engineering, University of Electronic Science and Technology of China (UESTC), Chengdu 611731, China; zhang_yong_ch@126.com; ychencd@uestc.edu.cn

2 Institute for Electric Vehicle Driving System and Safety Technology, Chengdu 611731, China

* Correspondence: zhang_yong_ch@126.com; Tel.: +86-028-66360106

Abstract: High step-up voltage gain nonisolated DC-DC converter have attracted much attention in photovoltaic, fuel cells and other renewable energy system applications. In this paper, by combining input current ripple-free boost cell with coupled-inductor voltage-doubler cell, an input current ripple-free high voltage gain nonisolated converter is proposed. In addition, passive lossless clamp circuit is adopted to recycle the leakage inductor energy and to reduce the voltage spike across the power switch. By utilizing voltage-doubler cell consisting of diode and capacitor, the voltage stress of switch is further reduced and the resonance between the leakage inductor and the stray capacitor of the output diode is eliminated. A low switch-on-resistance low-voltage-rated MOSFET can therefore be employed to reduce the conduction loss and cost. The reverse recovery loss of output diode is reduced, and the efficiency of converter can be improved. Furthermore, the proposed converter can achieve nearly zero input current-ripple and make the design of electromagnetic interference (EMI) filter easy. Steady state analysis and operation mode of the converter is performed. Finally, experimental results are presented to verify the analysis results of the proposed converter.

Keywords: input current ripple-free; boost converter; coupled-inductor; voltage-doubler cell; passive lossless clamp circuits; high voltage gain; renewable energy

1. Introduction

With the exhaustion of the global resources and the environmental pollution, the research on the renewable energy sources [1-7] such as fuel cells and photovoltaic cells has been gradually increased in industrial fields. Generally, the renewable energy sources generate low-voltage energy, thus power conditioning system (PCS) for renewable energy sources are required to regulate the output voltage for commercial, industrial, residential application. A typical renewable energy conversion system [8-10] is shown in fig.1, frond-end dc-dc converter is used to get high voltage dc bus for utility grid. In this application, Boost converter [11] can provide high dc voltage gain when operates at extremely high duty cycle, however, it increases the input current ripple of the converter, the conduction losses and the turned-off losses of power switch. Its transient response is also affected due to narrow turned-off time of power switches. In addition, output diode reverse-recovery problem is serious, which results in large conduction losses of power device and also increases the rating of power devices. Furthermore, the voltage stress of the power switch equals to the output voltage, and hence a high-voltage rating power switch with high on-resistance should be employed, generating high conduction losses. Consequently, the conversion efficiency is degraded and the electromagnetic interference (EMI) problem is severe under this situation.

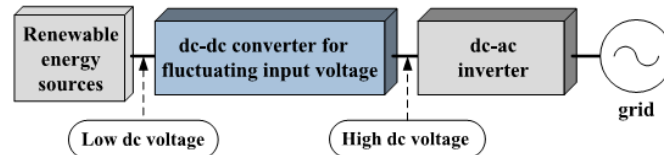


Fig. 1. Renewable energy conversion system.

To achieve a high conversion ratio and to avoid operating at extremely high duty cycles, many nonisolated converter topologies have been studied [1-6,8-18]. By using switched capacitor or switched inductor cell, high voltage gain of converter can be achieved [12-14]. However, it makes the switch suffer from high transient current and large conduction losses. Furthermore, many switched capacitor or switched inductor cells are indispensable to obtain extremely high step-up conversion, which increases the circuit complexity. Quadratic boost converter [15] using a single active switch is another interesting topology for extending the voltage gain, where the voltage conversion ratio is given as a quadratic function of the duty ratio. However, the voltage gain of this converter is moderately since the output voltage level is determined only by the duty cycle, and due to the cascade structure, it causes lower efficient of the converter.

The coupled inductor or isolated transformer-based converters [3,4,9,15-19] are other solutions to realize high step-up gain, where the turns ratio of the coupled inductor can be employed as a design freedom to extend the voltage gain. However, the inherent leakage inductance of the coupled inductor may not only cause high voltage spikes across the switch when it is turned off, but also produce large energy losses. A resistor-capacitor-diode (RCD) snubber circuit can suppress the voltage stress of the power switch, but the leakage energy is dissipated. Also, active clamp scheme or passive clamp circuit are utilized to recycle the leakage inductor energy and absorb voltage spike of the power switch [18]. Unfortunately, the input current of coupled inductor-based converter is discontinuous. Specially, as the turn ratio of the coupled-inductor or tapped-inductor is increased to extend the voltage conversion ratio, the input current ripple becomes larger.

Actually, current harmonics in fuel cell stack or photovoltaics makes the control of maximum efficiency point difficult, and also generates excessive losses and overheating [20,21], i.e. input current ripple of power converter greatly impact its power conversion efficiency. Thus, high boost-ratio converters with continuous input current are highly preferred. Current-fed converter exhibits continuous input current and boost-ratio gain characteristics, reducing the input filter capacitor and conduction loss, thereby enhancing the performance of the converter. By using a mirror ripple circuit, a zero input current ripple Boost converter for fuel cell applications is proposed in [22], however, additional active switch is required, which increases the complexity of the converter. The transformer-less high-gain boost converter proposed in [23] can achieve input current ripple cancelation at a selectable duty cycle. A passive ripple cancelling circuit is proposed in [24]-[26], however, it increase design complexity of magnetic component.

In this paper, a zero input current ripple high voltage gain nonisolated DC-DC converter is presented. By using coupled-inductor cell, high voltage gain of the proposed converter is achieved by adjusting turns ratio of coupled-inductor. To relieve voltage spikes of the power switch induced by leakage inductor of coupled inductor, a passive lossless snubber circuit with a diode and a capacitor is utilized, and the leakage inductor energy is also recycled. In addition, voltage-doubler cell is used to further extend voltage gain of converter to avoid operating at extremely duty cycle. Furthermore, voltage oscillations of the output diode due to resonance of parasitic capacitance of output diode and secondary leakage inductance of coupled inductor are eliminated.

The paper is organized as follows. In Section 2, operating mode of the proposed converter is discussed. The operating characteristics analysis, i.e. the condition of input current ripple-free, the input-output voltage gain ratio, the voltage stress, and the performance comparison, are performed in Section 3. Experimental results are given in Section 4 and the conclusion is given in Section 5.

2. Operating principle of the proposed converter

2.1. Circuit description

Fig. 2(a) shows the proposed input current ripple-free high voltage gain nonisolated converter with voltage-doubler cell and coupled inductor, with its corresponding equivalent circuit as shown in Figure 2(b). In Fig.2 (b), the coupled inductor is modeled by an ideal transformer with turns ratio of $n_p: n_s = 1:n$, a magnetizing inductor L_m and a leakage inductor L_s . Passive lossless clamp circuit, consisting of diode D_c and capacitor C_c , is utilized to recycle leakage inductor energy and absorb voltage spike of switch S_1 when switch S_1 is turned-off. The coupled inductor voltage-doubler cell consists of secondary of ideal transformer, capacitor C_2 , and regenerative diode D_1 . The voltage-doubler cell, consisting of capacitor C_2 and diode D_1 , can further enhance the voltage gain and reduce voltage stress across switch S_1 and output diode D_o . C_1 is intermediate storage capacitor, L_a is input filter inductor, C_o is output filter capacitor and R_o is load resistance. To simplify the analysis, following assumptions are made:

- a) Power switch S_1 is ideal except its anti-paralleled diode and output capacitor;
- b) Capacitors C_1 , C_2 and C_o are so large that voltages V_{C1} , V_{C2} and V_o can be considered as constants in a switching cycle.

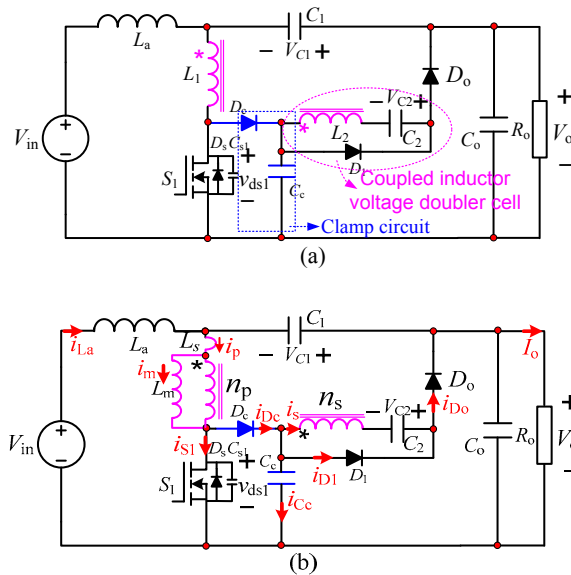


Fig. 2 Zero input current ripple high voltage gain converter

2.2 Operating Mode Analysis

Fig. 2(a) shows the proposed input current ripple-free high voltage gain nonisolated converter with voltage- There are seven main subintervals during one switching cycle. The key waveforms are shown in Fig. 3 and the corresponding equivalent circuits for each operation mode are shown in Fig. 4. At the beginning of each switching cycle, magnetizing inductor current i_m is greater than zero and output diode D_o is conducted to provide freewheeling current path.

Mode 1 [$t_0 \sim t_1$]: At t_0 , driving pulse V_{gs1} is applied to switch S_1 , the parasitic capacitor of switch S_1 resonates with leakage inductor of coupled-inductor to discharge energy to the load through capacitor C_1 . Output diode D_o is conducted to provide the path for magnetizing inductor current i_m . Diode D_c is turned off and capacitors C_c and C_2 transfer energy to the load through output diode D_o . The time interval of this mode is very short as capacitance of C_{s1} is very small.

Mode 2 [$t_1 \sim t_2$]: At t_1 , parasitic capacitor of switch S_1 is discharged completely and S_1 is turned on. At the same time, current flowing through output diode D_o is great than zero and D_o is still conducting. This mode ends when the current i_{D_o} flowing through output diode decreases to zero.

Mode 3 [$t_2 \sim t_3$]: At time t_2 , output diode current i_{D_o} falls to zero, and output diode D_o is turned off at zero current. At the same time, the secondary current of coupled-inductor i_s decreases to zero and

diode D_1 is turned on to provide current flowing path for i_s . Secondary voltage of coupled-inductor is clamped to V_{C2} , magnetizing inductor current i_m increases linearly

$$i_m(t) = i_m(t_2) + \frac{V_{C2}}{nL_1}(t - t_2) \quad (1)$$

where n is turns ratio of coupled inductor. Leakage inductor current i_p is equal to the current flowing through switch S_1

$$i_{S1}(t) = i_p(t) = i_p(t_2) + \frac{V_o - V_{C1} - V_{C2}/n}{L_s}(t - t_2) \quad (2)$$

Secondary current of coupled-inductor can be expressed as

$$i_s(t) = -i_{D1}(t) = \frac{i_m(t) - i_p(t)}{n} \quad (3)$$

Mode 4 [$t_3 \sim t_4$]: At time t_3 , switch S_1 is turned off, parasitic capacitor of switch S_1 is charged and the voltage across power switch increases, and secondary current i_s continues flowing through diode D_1 . When switch current i_{S1} decrease to zero, this mode ends. The time interval in this mode is very short due to small capacitance of C_{S1} .

Mode 5 [$t_4 \sim t_5$]: At t_4 , capacitor C_{S1} is charged completely and switch S_1 is turned off. In order to provide flowing path for leakage inductor current i_p , diode D_c is turned on. At the same time, capacitor C_c is charged by i_p . Leakage inductor current i_p decreases linearly

$$i_{Dc}(t) = i_p(t) = i_p(t_4) - \frac{V_{C1} + V_{Cc} + V_{C2}/n - V_o}{L_s}(t - t_4) \quad (4)$$

Voltage V_{C2}/n is applied to inductor L_1 , which makes i_m increase. The current flowing through the secondary side of coupled inductor decreases rapidly. When diode current i_{D1} decreases to zero, this operation mode ends.

Mode 6 [$t_5 \sim t_6$]: At t_5 , i_{D1} decreases to zero, and diode D_1 is turned off at zero current, which eliminates the reverse recovery losses of diode D_1 . At the same time, i_s increases to zero and continue to increase, output diode D_o is conducted to provide current flowing path of i_s . Leakage inductor releases energy to capacitor C_c through diode D_c . Secondary voltage of coupled inductor is clamped at $V_{C1} + V_{C2} - V_o$, magnetizing inductor current i_m and leakage inductor current i_p can be expressed as

$$i_m(t) = i_m(t_5) - \frac{V_o - V_{C1} - V_{C2}}{nL_1}(t - t_5) \quad (5)$$

$$i_p(t) = i_p(t_5) - \frac{V_{C1} + V_{Cc} + (V_{C2} - V_o)/n - V_o}{L_s}(t - t_5) \quad (6)$$

When leakage inductor current i_p decreases to zero, this mode ends.

Mode 7 [$t_6 \sim t_7$]: At t_6 , leakage inductor current i_p decreases to zero, and then capacitor C_c in series with capacitor C_2 transfer energy to the load through output diode D_o . Primary magnetizing inductor current i_m is freewheeled through the secondary side of coupled inductor, diode D_o , and capacitors C_c and C_2 . Magnetizing inductor current i_m decreases linearly until the beginning of next switching cycle.

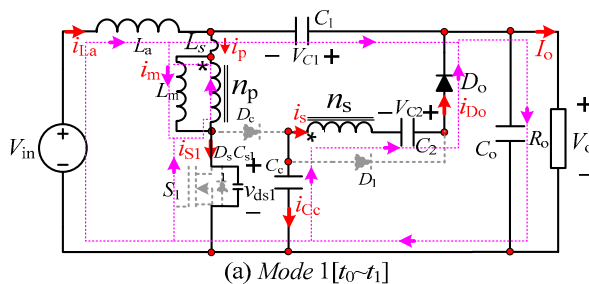


Fig. 3 Operation modes of the proposed converter

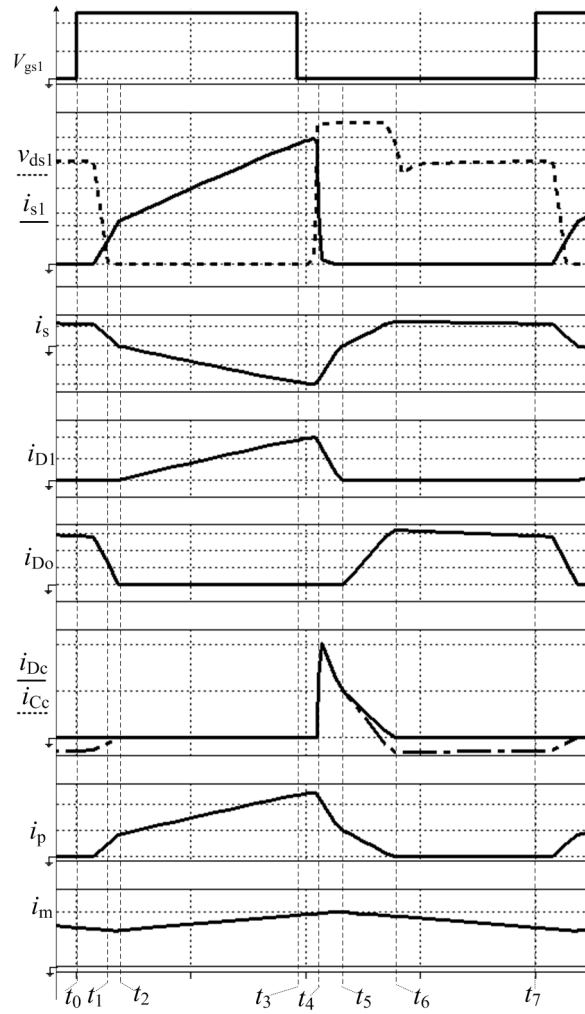


Fig. 4 Typical waveforms of the proposed converter

3. Performance Analysis

3.1. Condition of ripple-free input current

According to above operation mode analysis in one switching cycle, voltage across input filter inductor L_a can be expressed as

$$V_{La} = L_a \frac{di_{La}(t)}{dt} = V_{in} - V_o + V_{C1} \quad (7)$$

As intermediate storage capacitor C_1 and output filter capacitor C_o are so large that their ripple voltages can be neglected, the voltages across C_1 and C_o can be considered as constant in one switching cycle. Therefore, the voltage across inductor L_a is almost constant. Furthermore, in order to achieve ripple-free zero input, inductor current i_{La} should remain constant, i.e. $di_{La}/dt=0$, in this case, the voltage across intermediate capacitor C_1 can be expressed as

$$V_{C1} = V_o - V_{in} \quad (8)$$

As long as eq. (8) is satisfied, ripple-free input current of the proposed converter can be achieved. It can be seen that for the proposed converter, the ripple-free input current has no relation with the other circuit parameters and the duty cycle [25,26]. Furthermore, the proposed converter has only one power switch, without increases the cost and control complexity. To achieve ripple-free input current, only larger capacitance of capacitor C_1 is required.

3.2. Voltage Gain

It can be seen from above analysis that the time interval of mode 1, 2 and mode 4, 5 are so short that their effects on the proposed converter can be ignored in steady-state analysis. Fig. 5 shows the simplified key waveforms, where D is duty cycle of switch S_1 , D_1 is duty cycle of diode D_c and T_s is switching period.

During on-state interval of switch S_1 , inductor L_m is in series with leakage inductor L_s . Let $k = L_m / (L_s + L_m)$, then the voltage across inductor L_m is

$$v_{L1} = kV_{in} \quad (9)$$

Moreover, the voltage across the secondary winding of the ideal transformer can be represented as

$$v_{L2} = nv_{L1} = nkV_{in} \quad (10)$$

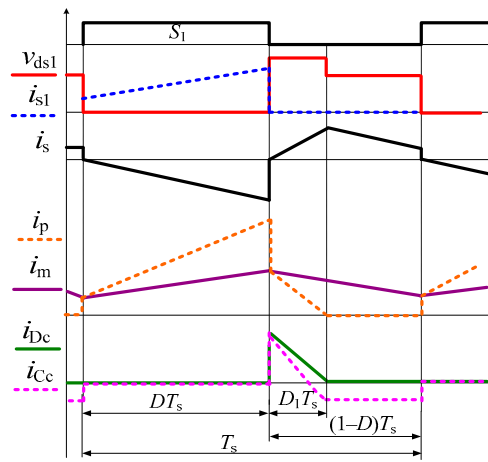


Fig. 5 Simplified waveforms of the proposed converter.

When switch S_1 is turned on as shown in the mode 3, the voltage across the secondary winding of the ideal transformer equals to capacitor voltage V_{C2} , thus

$$v_{L2} = V_{C2} = nkV_{in} \quad (11)$$

When switch S_1 is turned off as shown in the mode 6, the voltages across magnetizing inductor can be denoted as

$$v_{L1} = k(V_{in} - V_{C2}) = \frac{V_{C2} + V_{C2} - V_o}{n} = \frac{V_{C2} - V_{C1}}{n+1} \quad (12)$$

When switch S_1 is turned off, diode D_c is turned on to provide current flowing path for leakage inductor current i_p , i.e. time interval $[t_4 \sim t_6]$ as shown in Fig.4. In this time interval, leakage inductor current i_p decreases linearly, and output diode current i_{Dc} increase linearly. When i_{Dc} increases to magnetizing inductor current i_m reflected to the secondary side of the coupled inductor, the energy stored in leakage inductor is released completely and diode current i_{Dc} decreases to zero. In the time interval $[t_6 \sim t_7]$, output diode current i_{Dc} equals to current flowing through capacitor C_c . the duty cycle of diode D_c can be expressed as

$$D_1 = \frac{2}{n+1}(1-D) \quad (13)$$

When switch S_1 is turned on, voltage across the primary inductor is V_{C2}/n ; the switch S_1 is turned off, magnetizing inductor voltage equals to $(V_{C2} + V_{C2} - V_o)/n$. According to volt-second balance of inductor L_m , it can be seen that

$$\frac{V_{C2}}{n} DT_s + \frac{V_{C2} + V_{C2} - V_o}{n} (1-D)T_s = 0 \quad (14)$$

From eqs. (8), (11), (12), (14), it can have

$$\begin{aligned} V_o &= \frac{nk+1}{1-D} V_{in}, & V_{C1} &= \frac{nk+D}{1-D} V_{in} \\ V_{Cc} &= \frac{1}{1-D} V_{in}, & V_{C2} &= nkV_{in} \end{aligned} \quad (15)$$

Thus the voltage gain of the converter can be expressed as

$$M = \frac{V_o}{V_{in}} = \frac{nk+1}{1-D} \quad (16)$$

Fig. 6 shows the voltage gain of the proposed converter with $k = 1$, and the turns ratio of the transformer as $n = 1, 3, 5$. From Fig. 6, with the increase of duty cycle D and transformer turns ratio n , the voltage gain of the converter increases. Fig.7 shows voltage gain of the proposed converter with different leakage inductance of coupled inductor. It can be seen from Fig.7 that with the increase of leakage inductance L_s the voltage gain of the converter decreases slightly.

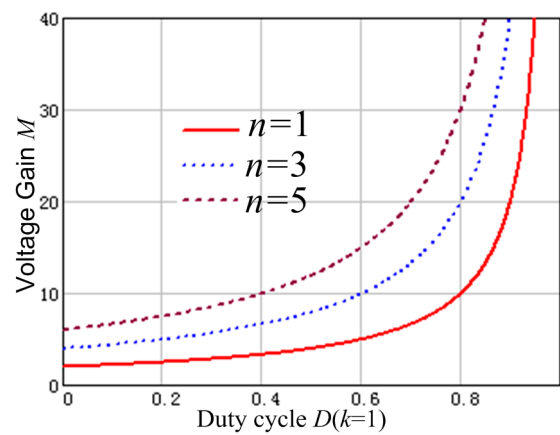


Fig. 6 Gain Curves of the proposed converter at $k=1$

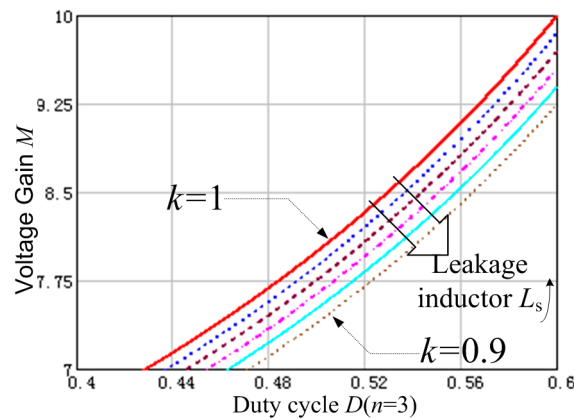


Fig. 7 Gain Curves of the proposed converter at $n=3$

3.3. Voltage Stress on Power Devices

From above operation mode analysis, it can be known that when switch S_1 is turned off, the voltage stress across power switch is clamped to V_{Cc}

$$V_{ds1,max} = V_{Cc} = \frac{1}{1-D} V_{in} \quad (17)$$

Voltage stress across diode D_o , D_1 , D_c can be obtained as

$$V_{D_o,max} = V_o - V_{Cc} = \frac{nk}{1-D} V_{in} \quad (18)$$

$$V_{D1,max} = V_{D0,max} = \frac{nk}{1-D} V_{in} \quad (19)$$

$$V_{Dc,max} = V_{Cc} = \frac{1}{1-D} V_{in} \quad (20)$$

Fig.8 shows normalized critical voltage stress of the proposed converter with input voltage V_{in} . From Fig.8, it can be seen that voltage stresses of switch S_1 , capacitor voltage C_1 , C_2 , and diode D_0 are lower than output voltage, although voltage stress of diode D_0 , D_1 is relate to transformer ratio n .

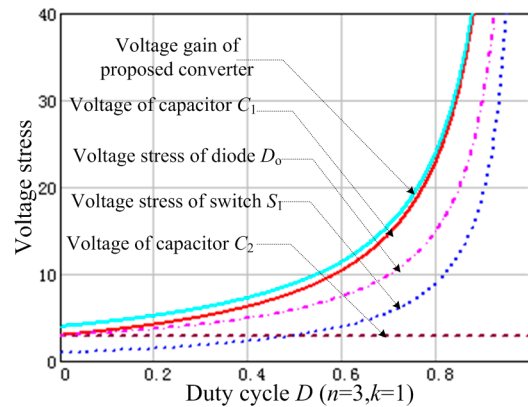


Fig. 8 voltage Stress of the proposed converter at $n=3$ and $k=1$

4. Experimental results

4.1. Design Example

In order to verify above analysis results, a experimental prototype is established with the key parameters of the converter as: output power $P_o = 80W$, input voltage $V_{in} = 24V$, output voltage $V_o = 200V$, input inductance $L_a = 50\mu H$, energy storage capacitor $C_1 = C_2 = C_c = 4.7\mu F$, output filter capacitor $C_o = 220\mu F$ and switching frequency $f_s = 100kHz$.

With these converter parameters, the voltage gain of the converter can be obtained as $V_o/V_{in} = 200/24 = 8.33$. As the leakage inductance will decrease the voltage gain of the converter, considering leakage inductance of coupled inductor is less than 5% of magnetizing inductance of the transformer, and high turns ratio produces higher voltage stress of output diode, design the turns ratio of transformer $n = 2.8$. According to eq.(16), duty cycle can be obtained as $D = 0.56$. The primary magnetizing inductance of the transformer is $L_1 = 40\mu H$, by selecting ETD34 core, primary and secondary turns ratio of 14T: 40T. Thus, the voltage stress of capacitor C_1 and C_2 can be given as $V_{C1} = 176V$, $V_{C2} = 72V$, and voltage stress of capacitor C_c as $V_{Cc} = 54.5V$. From eqs.(17)-(20), voltage stress of both diode D_1 and D_0 are 145V, voltage stress of the switch S_1 is 54.5V. Therefore, switch S_1 is a MOSFET STP19NF20 ($V_{DSS} = 200V$, $R_{DS(on)} = 0.16\Omega$), the diodes D_c are STPS3150, and the STTH302 is selected for D_1 and D_0 .

4.2. Experimental Results

Fig.9~Fig.16 show experimental results of the proposed converter at full load. Fig. 9 shows voltage and current waveforms of power switch S_1 . The voltage stress across the switch is about 56V. However, there exists small voltage spike across switch S_1 due to resonance of parasitic capacitance of the switch S_1 and diode D_c . Fig. 10 shows voltage and current waveforms of output diode D_0 , it can be seen that the voltage stress of output diode D_0 is clamped to 145V and voltage oscillations of diode voltage is eliminated. Fig.11 illustrates diode current i_{Dc} and the current flowing through capacitor i_{Cc} . Fig. 12 depicts leakage inductor current i_p and secondary current flowing through coupled inductor i_s . Figs. 13~16 show input current i_{La} , output voltage V_o and clamped capacitor voltage V_{Cc} , energy-storage capacitor voltage V_{C1} , capacitor voltage V_{C2} , respectively. It can be seen

from Fig.13 that zero input current ripple of the proposed converter is nearly achieved. Also, the measured voltage stress in Fig.14~Fig.16 are consistent with the theoretical analysis.

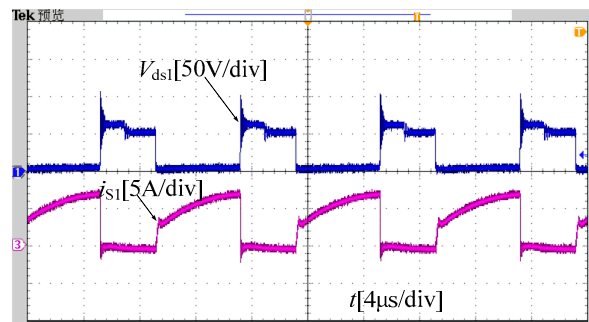


Fig. 9 Voltage and current switch S_1

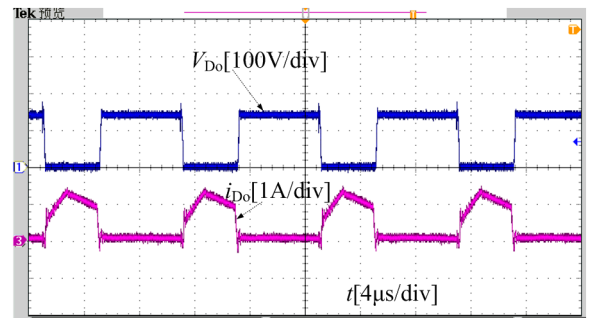


Fig. 10 Voltage and current of diode D_0

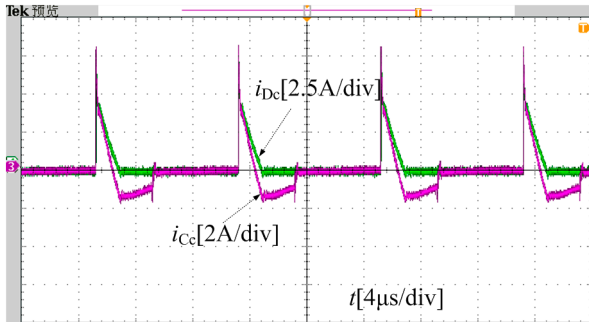


Fig. 11 current of passive lossless snubber D_c and C_c

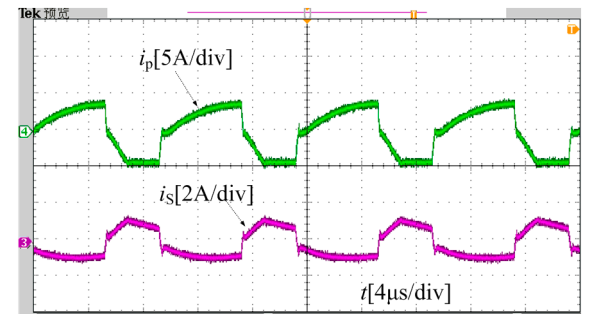


Fig. 12 Primary current of the coupled inductor

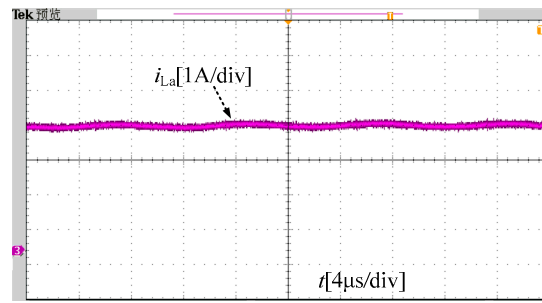


Fig. 13 Input current i_{La} flowing through inductor L_a

Fig.17 shows efficiency comparison of the proposed zero input current ripple high step-up voltage gain converter and the converter proposed in [12]. It can be seen from Fig.17, the proposed converter in this paper can achieve maximum efficiency of 94.5%, and 94% efficiency at full load. The coupled-inductor-based Boost converter proposed in [12] can achieve maximum efficiency of 93.5%. The power conversion efficiency improvement of the converter proposed in this paper is achieved due to following reasons: 1) by adjusting turns ratio of coupled-inductor, extreme duty cycle operation can be avoided in the converter proposed in this paper, therefore, improve the efficiency of the converter; 2) by utilizing voltage-doubler cell to extend the voltage gain, the voltage stress of switch is further reduced and the resonance between the leakage inductance and the stray capacitor of the output diode is eliminated. Thus, reverse recovery loss of the output diode D_o can be reduced to improve the efficiency of the converter. In addition, the proposed converter has zero input current ripple, which reduces design complexity of input filter.

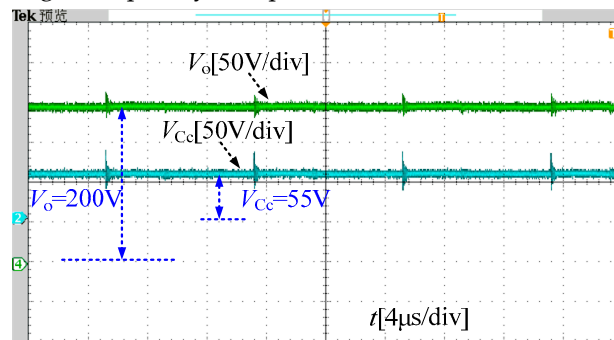


Fig. 14 Output voltage and clamped capacitor voltage

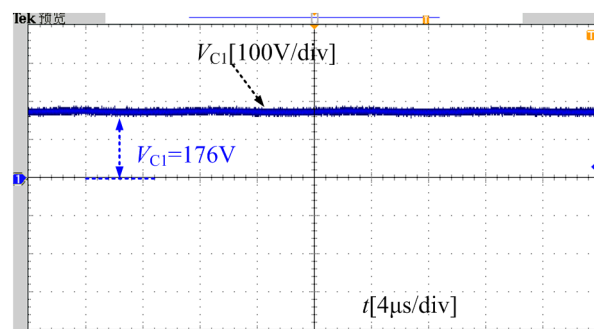


Fig. 15 Energy-storage capacitor voltage V_{C1}

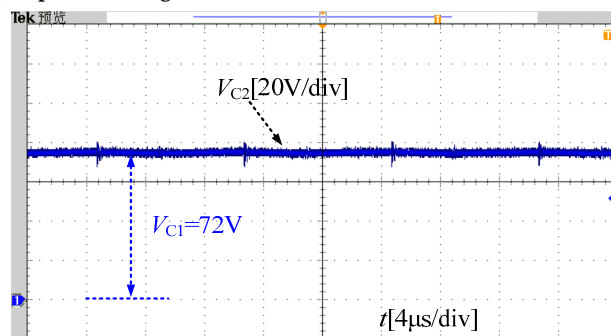


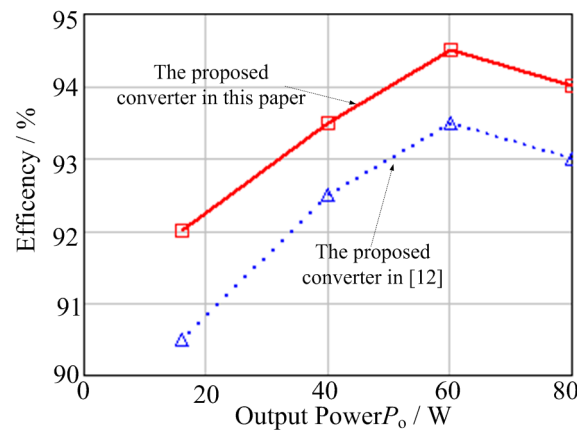
Fig. 16 Voltage waveform of capacitor C_2 

Fig. 17 Efficiency of experimental results

4. Conclusion

This paper presents an input current ripple-free high voltage gain nonisolated converter with coupled-inductor and voltage-doubler cell. The operating principle and operating characteristics of the proposed converter are analyzed in detail. Experimental results show that the proposed converter has inherent characteristic of zero input current ripple, and turns ratio of the coupled inductor can be employed as another design freedom to extend the voltage gain. Meanwhile, voltage stress of the switch is far less than output voltage, reduce cost and losses. Passive lossless snubber circuit can effectively recycle the leakage inductance energy and absorb voltage spike stress of the switch. In addition, resonance the parasitic capacitance of the output diode with the secondary side leakage inductance is eliminated by using voltage-doubler cell. Thus, the output diode voltage stress is reduced. Based on the above advantages, the proposed converter is suitable for photovoltaic, fuel cells applications.

Acknowledgments: This work was supported by the National Natural Science Foundation of China under grant no.51607027, the Fundamental Research Funds for the Central Universities under project number ZYGX2016KYQD123.

Author Contributions: Zhangyong chen conceived and designed the experiments, and analysis the results, Zhangyong chen and Yong chen wrote the paper. All authors have contributed to the editing and proofreading of this paper.

Conflicts of Interest: The authors declare no conflicts of interest.

References

1. Lu, X.; Wan, J. Modeling and control of the distributed power converters in a standalone DC microgrid. *Energies*, 2016, 9, 217.
2. B. R. Lin and J. Y. Dong. New zero-voltage switching DC-DC converter for renewable energy conversion systems. *IET Power Electron.*, 2012, 5, 393–400.
3. Tseng, Kuo-Ching, Jang-Ting Lin, and Chi-Chih Huang. High step-up converter with three-winding coupled inductor for fuel cell energy source applications. *IEEE Trans. Power Electron.*, 2015, 30, 574–581.
4. Tseng K C, Huang C C, Cheng C A. A High Step-Up Converter With Voltage-Multiplier Modules for Sustainable Energy Applications. *IEEE J. Emerg. Sel. Top. Power Electron.*, 2015, 3, 1100–1108.
5. Zhang, Longlong, et al. A high step-up DC to DC converter under alternating phase shift control for fuel cell power system. *IEEE Trans. Power Electron.*, 2015, 30, 1694–1703.
6. Ji F, Xiang J, Li W, et al. A Feedback Passivation Design for DC Microgrid and Its DC/DC Converters. *Energies*, 2016, 10, 14.
7. Zheng X, Ali H, Wu X, et al. Non-Linear Behavioral Modeling for DC-DC Converters and Dynamic Analysis of Distributed Energy Systems. *Energies*, 2017, 10, 63.
8. Sathyan, Shelas, et al. Soft-Switching DC-DC Converter for Distributed Energy Sources With High Step-Up Voltage Capability. *IEEE Trans. Ind. Electron.*, 2015, 62, 7039–7050.

9. Liu, Hong-Chen, and Fei Li. Novel High Step-Up DC–DC Converter With an Active Coupled-Inductor Network for a Sustainable Energy System. *IEEE Trans. Power Electron.*, 2015,30, 6476-6482.
10. Chen S M, Liang T J, Yang L S, et al. A safety enhanced, high step-up DC–DC converter for AC photovoltaic module application. *IEEE Trans. Power Electron.*, 2012, 27, 1809-1817.
11. Tofoli F L, de Castro Pereira D, de Paula W J, et al. Survey on non-isolated high-voltage step-up dc–dc topologies based on the boost converter. *IET Power Electron.*, 2015, 8, 2044-2057, .
12. Silva F.S.F, Freitas A.A.A., Daher S. et al, "High gain DC–DC boost converter with a coupling inductor," in *Proc. IEEE COBEP*, 2009, pp. 486–492.
13. B. Axelrod, Y. Berkovich, and A. Ioinovici. Switched capacitor/switched inductor structures for getting transformerless hybrid DC–DC PWM converters. *IEEE Trans. Circuits Syst. I, Reg. Papers*, 2008, 55, 687–696.
14. M. Prudente, L. L. Pfitscher, G. Emmendoerfer, E. F. Romaneli and R. Gules. Voltage Multiplier Cells Applied to Non-Isolated DC–DC Converters. *IEEE Trans. Power Electron.*, 2008, 23, 871-887.
15. Yang P, Xu J, Zhou G, et al. A new quadratic boost converter with high voltage step-up ratio and reduced voltage stress. in *Proc. IEEE IPEDMC*, 2012, 2, 1164-1168.
16. Lai C M, Pan C T, Cheng M C. High-efficiency modular high step-up interleaved boost converter for DC-microgrid applications. *IEEE Trans. Ind. Appl.*, 2012, 48, 161-171.
17. Tseng K C, Tsai M H, Chan C Y. Design of high step-up conversion circuit for fuel cell power supply system. in *Proc. IEEE ISNE*, 2013, pp. 506-509.
18. T.-F. Wu, Y.-S. Lai, J.-C. Hung, and Y.-M. Chen. Boost converter with coupled inductors and buck-boost type of active clamp. *IEEE Trans. Ind. Electron.*, 2008, 55, 154–162.
19. W. Li, X. He,. Review of Non-Isolated High Step-Up DC/DC Converters in Photovoltaic Grid-Connected Applications. *IEEE Trans. Ind. Electron.*, 2011, 58, 1239-1250.
20. N. D. Benavides and P. L. Chapman. Modeling the effect of voltage ripple on the power output of photovoltaic modules. *IEEE Trans. Ind. Electron.*, 2008, 55, 2638–2643.
21. G. Fontes, C. Turpin, S. Astier, and T. A. Meynard. Interactions between fuel cells and power converters: Influence of current harmonics on a fuel cell stack. *IEEE Trans. Power Electron.*, 2007, 22, 670–678.
22. Ching-Tsai Pan, Shih-Kun Liang, Ching-Ming Lai. A Zero Input Current Ripple Boost Converter for Fuel Cell Applications by Using a Mirror Ripple Circuit. in *Proc. IEEE IPEDMC*, 2009, 787 – 793.
23. Rosas, J., Mancilla-David, F., Mayo-Maldonado, J., Gonzalez et al. A transformer-less high-gain boost converter with input current ripple cancelation at a selectable duty cycle. *IEEE Trans. Ind. Electron.*, 2012, 60, 4492-4499.
24. Pan C T, Cheng M C, Lai C M. Current Ripple-Free Module Integrated Converter (MIC) with More Precise Maximum Power Tracking Control for PV Energy Harvesting. in *Proc. IEEE PEDS*, 2013, 1328 – 1334.
25. Do H L. Improved ZVS DC-DC converter with a high voltage gain and a ripple-free input current. *IEEE Trans. Circuits Syst. I, Reg. Papers*, 2012, 59, 846-853.
26. Do H L. Soft-Switching SEPIC Converter With Ripple-Free Input Current. *IEEE Trans. Power Electron.*, 2012, 27, 2879-2887.



© 2017 by the authors; licensee *Preprints*, Basel, Switzerland. This article is an open access article distributed under the terms and conditions of the Creative Commons by Attribution (CC-BY) license (<http://creativecommons.org/licenses/by/4.0/>).